

WEST VIRGINIA UNIVERSITY
College of Engineering

Aerospace
Engineering
TR-19

AD704502

OPTIMUM LOADING ON NONPLANAR WINGS
AT MINIMUM INDUCED DRAG

John L. Loth and Robert E. Boyle

August 1969

Project THEMIS
Prepared Under Contract
N00014-68-A-1512

for the

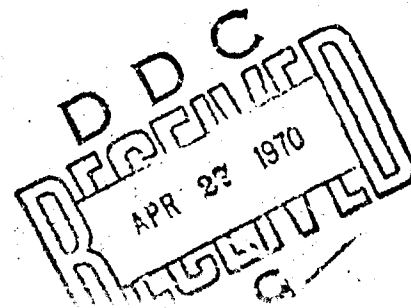
Office of Naval Research
Aeronautics, Code 461
(NR 215-163)

Reproduction in whole or in part is permitted for
any purpose of the United States Government.

This document has been approved for public release
and sale; its distribution is unlimited.

West Virginia University
Department of Aerospace Engineering
Morgantown, West Virginia

CLEARINGHOUSE



PREFACE

The results of this research were obtained by Dr. J. L. Loth, Associate Professor of Aerospace Engineering and Mr. R. E. Boyle, graduate research assistant of Aerospace Engineering at West Virginia University.

The authors wish to express their gratitude to Dr. P.B.S. Lissaman, Director, Continuum Mechanics Laboratory, Northrop Corporation, California, and Dr. A.I. van de Vooren, Chairman of the Department of Mathematics, University of Groningen, the Netherlands, for their valuable comments and suggestions.

SUMMARY

A numerical technique has been developed to compute the optimum spanwise load distribution on nonplanar wings of arbitrary shape. Complex curved wing configurations with multiple fences can be analyzed with this technique. M. M. Munk's criterion for minimum induced drag was used. The problem is solved in the two-dimensional Trefftz plane. The two-dimensional shed vortex sheet is assumed to have the same shape as the nonplanar wing, from which it has been shed.

J. L. Lundry of the McDonnell Douglas Corporation found an ingenious solution to this problem by computing the potential flow field, which would satisfy Munk's criterion. Lundry's method requires a Schwartz-Christoffel conformal transformation.

The method developed in this paper is different in that the numerical technique does not require a conformal transformation. The vortex sheet in the Trefftz plane is subdivided into $2N$ segments. Each vortex sheet segment is assumed to have a linear vorticity distribution. The velocity induced at $N-Q$ stations is determined with the Biot-Savart law. Because of symmetry it is sufficient to compute the velocities in one half of the vortex sheet. A set of $N-Q$ equations has been derived with as many unknowns. The unknowns are the strength of the shed vortex sheet at $N-Q$ stations. Munk's criterion provides the condition matrix for the magnitude of the normal component of the induced velocity. The strength of the shed vortex sheet is integrated to obtain the optimum spanwise loading on the nonplanar wing.

The technique has been tested on nonplanar wings with various dihedral angles and locations of the nonplanar wing sections. The nonplanar wing results are presented relative to those of a planar wing with elliptical loading. Both wings elected have identical lift and total wing peripheral length, and thus equal skin friction drag. It is shown that the ratio of the induced drag of the planar wing to that of the nonplanar wing is always less than one. The results are in complete agreement with those obtained by Lundry. However, because Lundry compared wings with equal span instead of equal peripheral length, he found this ratio to be always greater than 1.0.

In conclusion it can be said that if the span is the limiting factor it may be advantageous to use nonplanar wings with dihedral angle and fences. However if the wing peripheral length is limited, then the planar wing is always the most desirable configuration, with the highest lift over drag ratio.

TABLE OF CONTENTS

	Page
PREFACE	ii
SUMMARY	iii
SYMBOLS	vi
INTRODUCTION	1
METHOD OF ANALYSIS	5
RESULTS	19
CONCLUSIONS	29
REFERENCES	30
APPENDIX A	31
APPENDIX B	35
LIBRARY CARD ABSTRACT	38

SYMBOLS

English Letters:

A,B,..K	abbreviations as defined in appendix
D_i	induced drag
h	variable along vortex sheet segment
k	induced drag efficiency factor
L	lift
N	total number of the vortex sheet segments
\bar{n}	unit normal vector
P	abbreviation as defined in the appendix
Q	total number of wing and fence tips on a semispan
\vec{R}	radius vector
\vec{r}	radius vector
S	abbreviation as defined in the appendix
T	ratio as defined in Eq. (27)
w	downwash velocity
x,y	coordinates of the vortex sheet segments
\bar{z}	unit vector in downstream direction

Greek Letters:

α	coefficient defined in Eq. (11)
β	coefficient defined in Eq. (30)
Γ	bound vortex strength
Υ	shed vortex sheet strength
ψ	angle defined in Fig. 4

SYMBOLS (cont'd)

Θ	dihedral angle
η	non-dimensional spanwise coordinate
ρ	air density

Superscripts:

'	indicates the side of the vortex sheet at which the downwash is computed
"	indicates opposite side of the vortex sheet from where the downwash is computed
*	properties of a planar, elliptically loaded wing

Subscripts:

j	indicates anyone of the Q tip sections on the semispan
m	indicates the location of the inducing vortex sheet segment
n	indicates the location at which the induced velocity is computed
o	indicates the vortex sheet centerline conditions

INTRODUCTION

A progressively increasing need is becoming apparent for aircraft with STOL capabilities. The forty plus versions of fixed wing aircraft existing today, with both VTOL and STOL capabilities, represent a bare initial effort to satisfy both commercial and military requirements. Commercial needs include downtown-to-airport transportation, while those of the military are for operations from short runways such as those found on aircraft carriers.

STOL capability requires unusual wing configurations, often using multiple leading edges and trailing edge flaps with boundary layer control to obtain high lift coefficients. These modifications often require many fences to separate wing sections with different lift coefficients. The frequent use of horizontal or vertical engine nacelles adds further to the nonplanar nature of the wings. Aircraft on Naval carriers can benefit from a nonplanar wing configuration so as to reduce their required span and permit compact storage.

The computer technique developed in this paper calculates the optimum loading on any nonplanar wing of given complex geometry for the minimum lift over drag ratio. Such a computer program can be used to determine the effect of size, location, and dihedral angle of the fences employed on the overall lift to induced drag ratio of the wing. The computed optimum loading can determine the desired wing twist and taper.

The optimization technique is based on Munk's¹ criterion for minimum induced drag. This criterion requires that the cosine of the local dihedral angle equal the normal component of the local induced velocity divided by a constant.

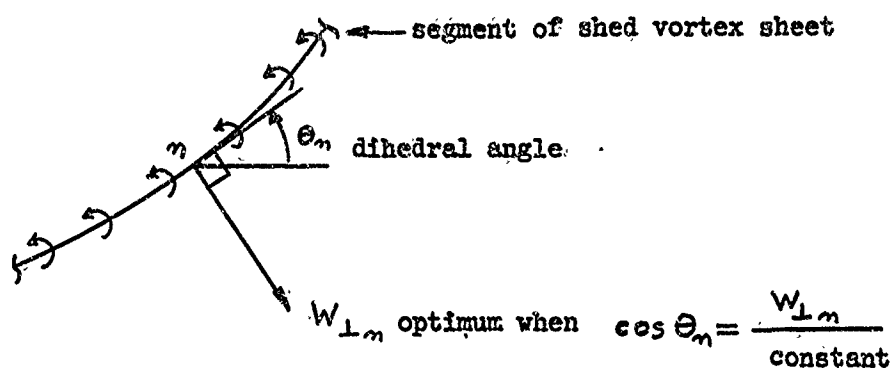


Figure 1: Munk's criterion for minimum induced drag.

For all planar wings, regardless of taper, aspect ratio, or sweep, the optimum spanwise loading is elliptical.

Because the induced drag of a wing is only a function of its spanwise loading and not of the aspect ratio it is desirable to derive the optimum spanwise loading in the Trefftz plane, which is located infinitely far downstream of the wing, where all chordwise effects can be ignored. The two-dimensional Trefftz plane is perpendicular to the double-infinite shed vortex sheet, which is assumed to remain undistorted and to maintain the same nonplanar shape as the wing.

¹Superscript numbers denote references.

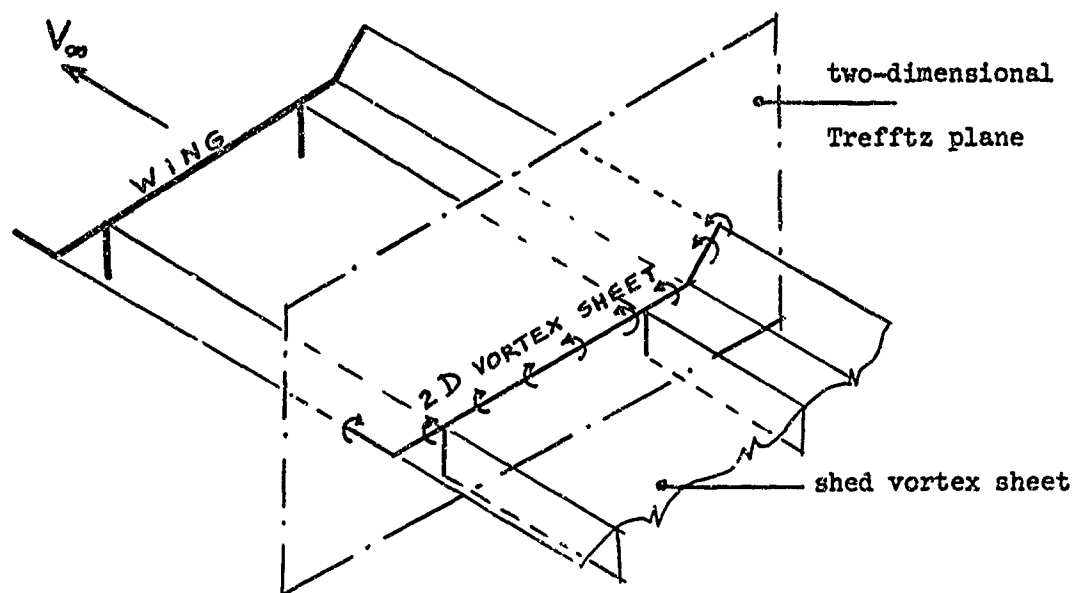


Figure 2: Schematic view of the Trefftz plane.

Lundry² has presented a solution to this problem by computing the potential flow field which satisfies Munk's criterion. By superimposing a uniform crossflow on the two-dimensional vortex sheet, he cancelled all the normal components of the downwash velocity and thus satisfied the boundary conditions on a solid surface. Next he computed the velocity potential around a solid surface in the shape of the nonplanar wing by using a Schwartz-Christoffel conformal mapping technique. Then by subtracting the velocity potential of the superimposed crossflow, he found the desired velocity potential of the induced velocities. The strength of the shed vortex sheet was found from the difference in the upper and lower tangential velocity components. Using integration, he subsequently computed the optimum spanwise loading on the wing.

The velocity past a solid surface in the shape of the nonplanar wing is zero at stagnation points, e.g., the root of a fence on the wing, and is infinite for the flow along the wing where there is a discontinuity in the dihedral angle, such discontinuities will be referred to as bends. Consequently Lundry's analysis shows that the strength γ of the vortex sheet segment shed by the fence is zero at the fence root. In addition a vortex sheet segment shed by either the top of a wing, fence, or by the bend in the wing, has infinite vorticity. Such segments require special treatment in a numerical calculation.

Lundry's analysis covers straight line segments because of the nature of the Schwartz-Christoffel transformation, but others³ have used mappings which have transformed curved lines to straight lines and performed a similar analysis. In references 2 and 3, the analysis was performed in the Trefftz plane and an undistorted wake assumption was made. A recent publication by Blackwell⁴ describes a numerical technique which does not use conformal mapping. His technique is a special form of lifting surface theory, which provides information on both the spanwise and chordwise optimum loading. Experimental work on nonplanar wings has been reported by Roberts⁵.

METHOD OF ANALYSIS

The vortex sheet shed by a given wing, with arbitrary shape and number of fences, is assumed to extend to infinity without any distortion. Only wings with an optimum loading will have a trailing vortex sheet which satisfies Munk's criterion at any spanwise location:

$$\cos \Theta_n = \frac{W_{L_n}}{W_0 = \text{constant}} \quad (1)$$

This criterion can be applied to the spanwise direction at the wing or at any other normal surface downstream of the wing. If the normal surface is chosen infinitely far downstream of the wing then one deals with the Trefftz plane and the problem has become two-dimensional. The velocities found in the Trefftz plane are induced by a two-dimensional double-infinite vortex sheet of strength γ . The shape of the shed vortex sheet is equal to that of the nonplanar wing, assuming an undistorted wake.

Identifying the semiwing total peripheral length by $\eta_{\max} = 1.0$ and the bound vorticity of the wing by $\Gamma = \Gamma(\eta)$, then the strength of the shed vortex sheet is:

$$\gamma = - \frac{d\Gamma}{d\eta} \quad (2)$$

NOT REPRODUCIBLE

If the semi-vortex sheet total peripheral length is γ_{max} divided into N segments of equal length $\Delta \gamma$ as shown in Fig. 3, then:

$$\Delta \gamma = \frac{\gamma_{max}}{N} \quad (3)$$

Define the number of wing and fence tips on the semispan as Q , and if each tip has $N(j)$ vortex sheet segments, where $1.0 \leq (j) \leq Q$, then the total number of vortex sheet segments is:

$$N = \sum_{j=1}^Q N(j) \quad (4)$$

An example is shown here with $Q = 5$ and $N = 26$.

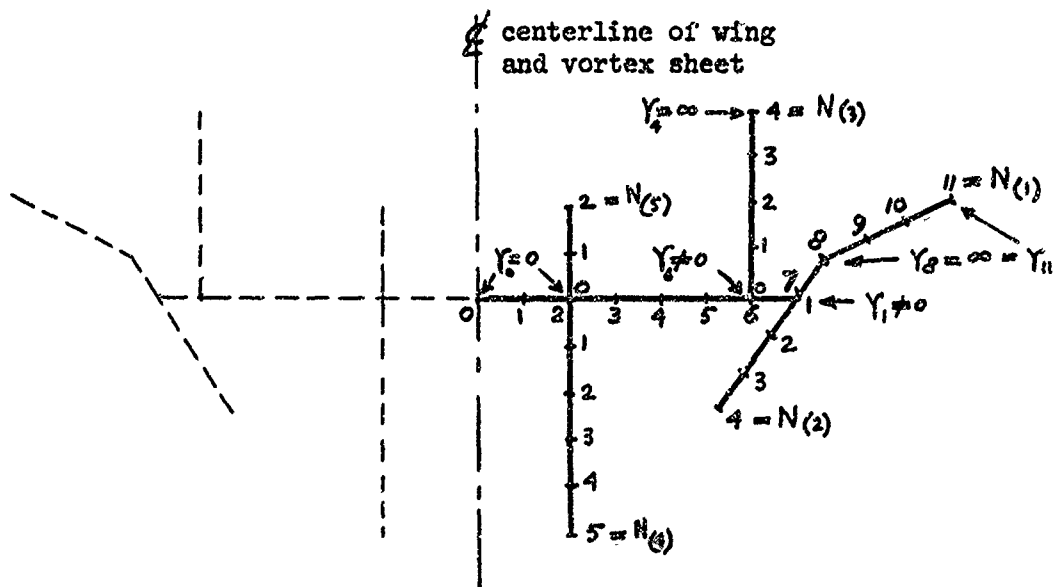


Figure 3: Example of an arbitrary nonplanar wing shape.

Munk's criterion will be satisfied at $N-Q$ stations $n_{(j)}$, where n varies from 1 through $N_{(j)}-1$. The $n_{(j)}$ stations are located on the right hand side of the vortex sheet; because Munk's criterion is automatically satisfied on the left hand side owing to symmetry.

The normal component of the velocity induced at $n_{(j)}$ by the entire shed double infinite vortex sheet is $W_{\perp n_{(j)}}$. This velocity component is composed of the sum

$$W_{\perp n_{(j)}} = \sum_{N_{(j)}=N_{(1)}}^{N_{(Q)}} \sum_{m_{(j)}=0}^{N_{(j)}-1} \Delta W_{\perp n_{(j)}, m_{(j)}} \quad (5)$$

where $\Delta W_{\perp n_{(j)}, m_{(j)}}$ is the velocity induced at $n_{(j)}$ by both the left hand and the right hand vortex sheet segments located between stations $m_{(j)}$ and $m_{(j+1)}$. The strength of these vortex sheet segments is: $+\gamma(\eta)$ for the right hand side and $-\gamma(\eta)$ for the symmetrically opposite segment on the left hand side. Using the Biot-Savart law and leaving off the subscript (j) gives

$$\Delta W_{\perp n, m} = \int_0^{\Delta\eta} \frac{\gamma}{2\pi(r'_{n,m})^2} \left[\vec{n} \cdot (\vec{r}'_{n,m} \times \vec{z}) \right] dh + \int_0^{\Delta\eta} \frac{-\gamma}{2\pi(r''_{n,m})^2} \left[\vec{n} \cdot (\vec{r}''_{n,m} \times \vec{z}) \right] dh \quad (6)$$

where:

- h is the running variable in the η direction having a maximum length $\Delta\eta$.
- \vec{z} is the unit vector in the downstream direction.
- \vec{n} is the unit vector normal to the vortex segment at point n .
- $\vec{r}'_{n,m}$ is the radius vector from n to the right hand vortex sheet segment at m .
- $\vec{r}''_{n,m}$ is the radius vector from n to the left hand vortex sheet segment at m .

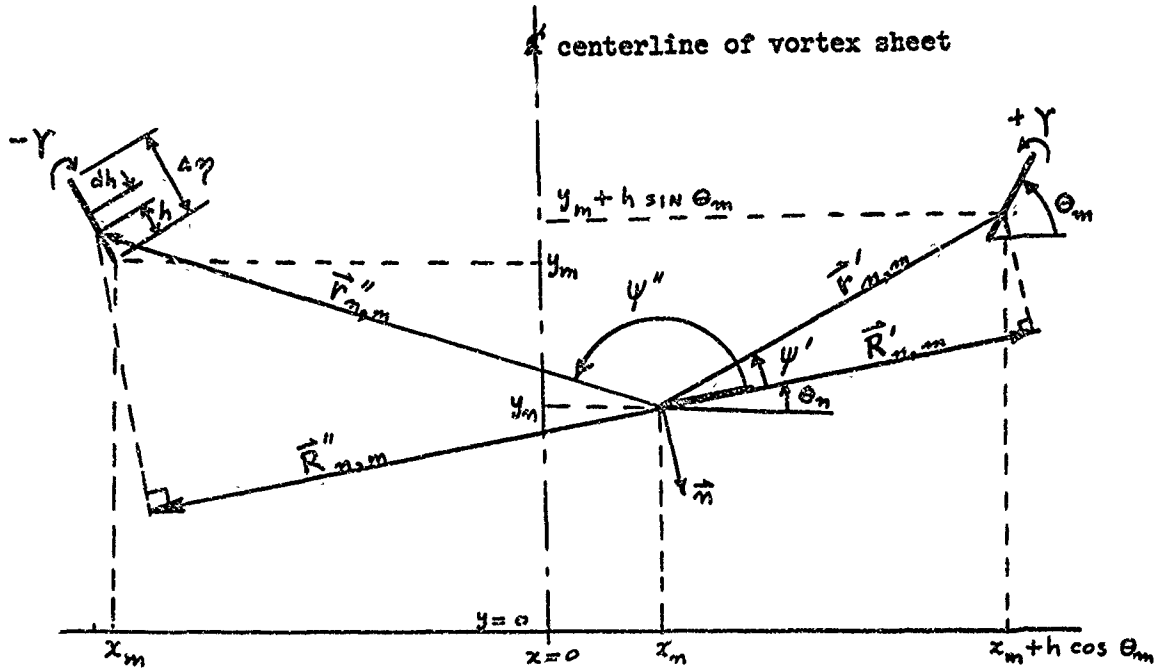


Figure 4: Schematic presentation of the geometry used in Eq.(6).

$$\Delta W_{\perp n,m} = \frac{1}{2\pi} \int_0^{\Delta\eta} \gamma \left[\frac{\cos \psi'}{r'_{n,m}} - \frac{\cos \psi''}{r''_{n,m}} \right] dh$$

$$\Delta W_{\perp n,m} = \frac{1}{2\pi} \int_0^{\Delta\eta} \gamma \left[\frac{R'_{n,m}}{(r'_{n,m})^2} - \frac{R''_{n,m}}{(r''_{n,m})^2} \right] dh \quad (7)$$

Where r and R can be expressed as functions of the known coordinates of the vortex sheet segments:

$$R'_{n,m} = (x_m + h \cos \theta_m - x_n) \cos \theta_n + (y_m + h \sin \theta_m - y_n) \sin \theta_n \quad (8a)$$

$$R''_{n,m} = (-x_m - h \cos \theta_m - x_n) \cos \theta_n + (y_m + h \sin \theta_m - y_n) \sin \theta_n \quad (8b)$$

R is positive for $\psi < \left| \frac{\pi}{2} \right|$ and negative for $\psi > \left| \frac{\pi}{2} \right|$
while r^2 is positive and can be written as:

$$(r'_{n,m})^2 = (x_m + h \cos \theta_m - x_n)^2 + (y_m + h \sin \theta_m - y_n)^2 \quad (9a)$$

$$(r''_{n,m})^2 = (-x_m - h \cos \theta_m - x_n)^2 + (y_m + h \sin \theta_m - y_n)^2 \quad (9b)$$

To be able to integrate Eq. (7) one has to assume a vortex distribution along the segment. Good accuracy has been obtained by assuming a linear vortex distribution, so that γ becomes a function of the two unknown values at the ends of each segment γ_m and γ_{m+1} :

$$\gamma = \gamma_m + \frac{h}{\Delta \eta} (\gamma_{m+1} - \gamma_m) \quad (10)$$

Combining Eqs. (7) and (10) gives

$$\Delta W_{\perp n,m} = Y_m(\alpha_{1n,m} + \alpha_{2n,m}) + (Y_{m+1} - Y_m)(\alpha_{3n,m} + \alpha_{4n,m}) \quad (11)$$

$$\alpha_{1n,m} = \frac{1}{2\pi} \int_0^{\Delta\eta} \frac{R'_{n,m}}{(r'_{n,m})^2} dh \quad (12)$$

$$\alpha_{2n,m} = \frac{1}{2\pi} \int_0^{\Delta\eta} \frac{-R''_{n,m}}{(r''_{n,m})^2} dh \quad (13)$$

$$\alpha_{3n,m} = \frac{1}{2\pi} \int_0^{\Delta\eta} \frac{h}{\Delta\eta} \left[\frac{R'_{n,m}}{(r'_{n,m})^2} \right] dh \quad (14)$$

$$\alpha_{4n,m} = \frac{1}{2\pi} \int_0^{\Delta\eta} \frac{h}{\Delta\eta} \left[\frac{-R''_{n,m}}{(r''_{n,m})^2} \right] dh \quad (15)$$

Equations (12-15) are integrated as shown in appendix A to give

$$\alpha_{1n,m} = \frac{1}{2\pi} \left[P \left(A - \frac{BF}{2} \right) + \frac{B}{2} \ln \left| \frac{1}{GN^2} + \frac{F}{GN} + 1 \right| \right]_{n,m} \quad (16)$$

$$\alpha_{2n,m} = \frac{-1}{2\pi} \left[S \left(D - \frac{EJ}{2} \right) + \frac{E}{2} \ln \left| \frac{1}{KN^2} + \frac{J}{KN} + 1 \right| \right]_{n,m} \quad (17)$$

$$\alpha_{3n,m} = \frac{N}{2\pi} \left[\frac{P}{2} (BF^2 - 2BG - AF) + \left(\frac{A-BF}{2} \right) \ln \left| \frac{1}{GN^2} + \frac{F}{GN} + 1 \right| + \frac{B}{N} \right]_{n,m} \quad (18)$$

$$\alpha_{4n,m} = \frac{-N}{2\pi} \left[\frac{S}{2} (EJ^2 - 2EK - DJ) + \left(\frac{D-EJ}{2} \right) \ln \left| \frac{1}{KN^2} + \frac{J}{KN} + 1 \right| + \frac{E}{N} \right]_{n,m} \quad (19)$$

The symbols A, B, C, etc., are functions of the known coordinates and dihedral angles of the vortex sheet segments (see Eqs. (38-47) in Appendix A). Equations (16-19) are the general forms of the coefficients in Eq. (11) except for the special case that $m = n-1$ or $m = n$. For $m = n$ one finds $\alpha_{1, n, m} = \infty$ and for $m = n-1$ one finds $\alpha_{1, m, m} = -\infty$. This is easily understood when it is realized that under these special conditions the contribution of the right hand side of the vortex sheet $\left[\Delta W_{\perp, m, m=n-1} \right]_{\alpha_1, \alpha_3}$ is computed at the end of vortex sheet segments of finite strength $\gamma_{m=n}$ and $\gamma_{m=n-1}$, and then the velocity becomes infinite. This problem can be avoided when $\left[\Delta W_{\perp, m, m=n-1} \right]_{\alpha_1, \alpha_3}$ is computed for both adjacent vortex sheet elements simultaneously as shown in Fig. 14 (see Appendix B). The results of such special treatment are:

$$\text{for } m = n-1 \quad \left\{ \begin{array}{l} \alpha_{1, n, m=n-1} = - \frac{\cos \frac{1}{2} (\theta_n - \theta_{n-1})}{2\pi} \quad (20) \\ \alpha_{3, n, m=n-1} = 0 \quad (21) \end{array} \right.$$

$$\text{for } m = n \quad \left\{ \begin{array}{l} \alpha_{1, m, m=n} = + \frac{\cos \frac{1}{2} (\theta_n - \theta_{n-1})}{2\pi} \quad (22) \\ \alpha_{3, m, m=n} = + \frac{\cos \frac{1}{2} (\theta_n - \theta_{n-1})}{2\pi} \quad (23) \end{array} \right.$$

These equations have been derived in appendix B (see Eqs. (53-56)).

Another difficulty arising in the application of Eq. (11) occurs when $m + 1 = N(j)$ or $\gamma_{m+1} = \gamma_{N(j)}$ which is the vorticity shed by either a wing tip or a fence tip. This vorticity is, of course, infinite and when used in Eq. (11) would make $\Delta W_{\perp n, m=N(j)-1} = \infty$. This problem has been overcome by assuming that γ shed by the non-planar wing goes to infinity at $N(j)$ at the same rate as the vorticity γ^* shed by an elliptically loaded planar wing becomes infinite at the edge. Defining the semispan of the planar wing by $\eta_N = 1.0$ and the strength of the bound vortex at the centerline by Γ_o^* gives:

$$\gamma^* = \Gamma_o^* \frac{\eta}{(1 - \eta^2)^{1/2}}$$

and γ_{N-2}^* at the distance $2 \Delta \eta$ from the edge is given by:

$$\gamma_{N-2}^* = \Gamma_o^* \frac{\eta_{N-2}}{(1 - \eta_{N-2}^2)^{1/2}} \quad \text{or} \quad \Gamma_o^* = \gamma_{N-2}^* \frac{(1 - \eta_{N-2}^2)^{1/2}}{\eta_{N-2}}$$

$$\gamma^* = \gamma_{N-2}^* \frac{(1 - \eta_{N-2}^2)^{1/2}}{\eta_{N-2}} \cdot \frac{\eta}{(1 - \eta^2)^{1/2}} \quad (24)$$

The normal component of the downwash velocity induced at station $N-1$, adjacent to the tip is most sensitive to the accuracy of the vorticity at the tip. If the downwash velocity at $N-1$, induced by the vortex sheet segment between $N-1$ and N is computed, the result will be infinite. This is because $\left[\Delta W_{\perp N-1} \right]_{\alpha_1, \alpha_3}$ is evaluated at the end of a vortex sheet with finite strength. However, if $\left[\Delta W_{\perp N-1} \right]_{\alpha_1, \alpha_3}$ is induced by both adjacent vortex sheet segments, then this normal velocity will be finite, as shown in Eq. (52) (see Appendix B).

One can compute $\left[\Delta W_{\perp N-1}^* \right]_{\alpha_1, \alpha_3}$ induced by the two adjacent segments of strength γ^* as shed by an elliptically loaded planar wing by:

$$\left[\Delta W_{\perp N-1}^* \right]_{\alpha_1, \alpha_3} = \int_{\gamma_{N-2}}^{\gamma_N} \frac{\gamma^* d\gamma}{2\pi(\gamma - \gamma_{N-1})} = \frac{\gamma_{N-2}^*}{2\pi} \frac{(1 - \gamma_{N-2}^2)^{1/2}}{\gamma_{N-2}} \int_{\gamma_{N-2}}^{\gamma_N} \frac{\eta d\eta}{(\eta - \gamma_{N-1})(1 - \eta^2)^{1/2}}$$

replace η by $\cos z$ and $d\eta$ by $-\sin z dz$

$$\left[\Delta W_{\perp N-1}^* \right]_{\alpha_1, \alpha_3} = \frac{\gamma_{N-2}^*}{2\pi} \cdot \frac{(1 - \gamma_{N-2}^2)^{1/2}}{\gamma_{N-2}} \int_{z_{N-2}}^0 \frac{-\cos z dz}{(\cos z - \cos z_{N-1})}$$

$$\left[\Delta W_{\perp N-1}^* \right]_{\alpha_1, \alpha_3} = \frac{\gamma_{N-2}^*}{2\pi} \cdot \frac{(1 - \gamma_{N-2}^2)^{1/2}}{\gamma_{N-2}} \left[\cos^{-1} \gamma_{N-2} + \frac{2\gamma_{N-1}}{(1 - \gamma_{N-1}^2)^{1/2}} \ln \left| \frac{(1 + \gamma_{N-1}) \left(\frac{1 - \gamma_{N-2}}{1 + \gamma_{N-2}} \right)^{1/2} + (1 - \gamma_{N-1}^2)^{1/2}}{(1 + \gamma_{N-1}) \left(\frac{1 - \gamma_{N-2}}{1 + \gamma_{N-2}} \right)^{1/2} - (1 - \gamma_{N-1}^2)^{1/2}} \right| \right] \quad (25)$$

Compare $\left[\Delta W_{\perp N-1}^* \right]_{\alpha_1, \alpha_3}$ to the expression found for the velocity induced by two adjacent vortex sheet segments with a linear vorticity distribution as was derived in Eq. (52) (see appendix B) and which is repeated here as:

$$\left[\Delta W_{\perp N(j)-1} \right]_{\alpha_1, \alpha_3} = \frac{\gamma_{N(j)-2}}{2\pi} \left[\left(\frac{\gamma_{N(j)}}{\gamma_{N(j)-2}} - 1 \right) \cos \frac{1}{2} (\Theta_{n(j)-1} - \Theta_{n(j)-2}) \right] \quad (26)$$

If the induced velocity $\left[\Delta W_{\perp N-1}^* \right]_{\alpha_1, \alpha_3}$ is set equal to $\left[\Delta W_{\perp N(j)-1} \right]_{\alpha_1, \alpha_3}$ and the vorticity γ_{N-2}^* equal to $\gamma_{N(j)-2}$ then an equivalent finite value for the tip vorticity $\gamma_{N(j)}$ is found as a function of the vorticity $\gamma_{N(j)-2}$.

Equating Eq. (25) to Eq. (26) gives the equivalent finite tip vorticity $\Upsilon_{N(j)}$ as:

$$\Upsilon_{N(j)} = T \cdot \Upsilon_{N(j)-2} \quad (27)$$

where T is given by:

$$T = \left[1 + \frac{(1 - \gamma_{N-2}^2)^{1/2}}{\gamma_{N-2} \cos \frac{1}{2}(\Theta_{N(j)-1} - \Theta_{N(j)-2})} \left\{ \cos^{-1} \gamma_{N-2} + \frac{2\gamma_{N-1}}{(1 - \gamma_{N-1}^2)^{1/2}} \times \right. \right. \\ \left. \left. \ln \left| \frac{(1 + \gamma_{N-1}) \left(\frac{1 - \gamma_{N-2}}{1 + \gamma_{N-2}} \right)^{1/2} + (1 - \gamma_{N-1})^{1/2}}{(1 + \gamma_{N-1}) \left(\frac{1 - \gamma_{N-2}}{1 + \gamma_{N-2}} \right)^{1/2} - (1 - \gamma_{N-1})^{1/2}} \right| \right\} \right] \quad (28)$$

Equation (28) is quite insensitive to the size of the increment used.

For example:

$$\Delta \gamma = 10^{-4} \quad \text{gives} \quad T = 5.986$$

$$\Delta \gamma = 10^{-3} \quad \text{gives} \quad T = 5.991$$

$$\Delta \gamma = 10^{-2} \quad \text{gives} \quad T = 6.044$$

$$\Delta \gamma = 10^{-1} \quad \text{gives} \quad T = 6.714$$

$$\gamma_{N-1} = \gamma_N - \Delta \gamma$$

$$\gamma_{N-2} = \gamma_N - 2 \Delta \gamma$$

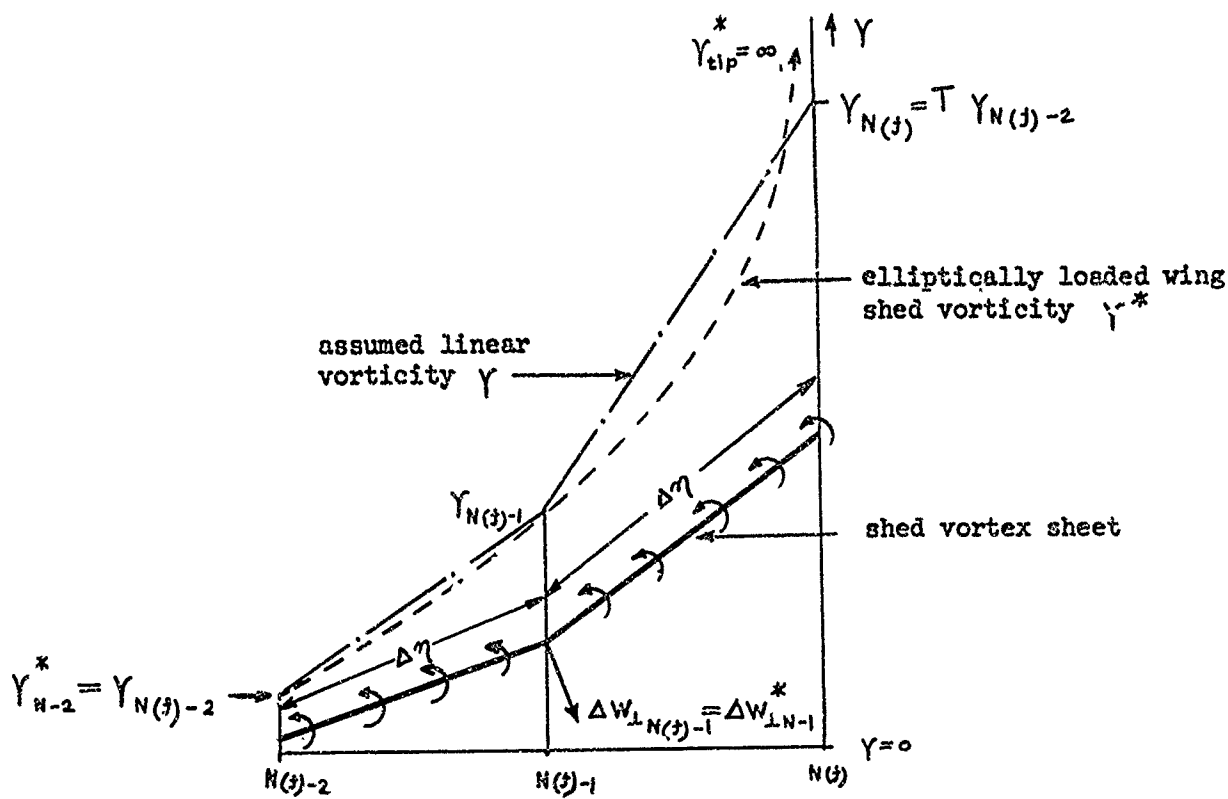


Figure 5: Graphical presentation of the finite tip strength approximation.

All the terms in Eq. (11) have now been defined and the next step is to solve the optimum vorticity distribution in the shed vortex sheet.

Applying Munk's criterion from Eq. (1) gives:

$$\cos \Theta_{n(j)} = \frac{W_{\perp n(j)}}{W_0} = \sum_{N(j)=N(i)}^{N(j)} \sum_{m(j)=0}^{N(j)-1} \frac{\Delta W_{\perp n(j) > m(j)}}{W_0}$$

Using the expression for the induced velocity from Eq. (11) gives:

$$\cos \Theta_{n(j)} = \sum_{N(j)=N(i)}^{N(j)} \sum_{m(j)=0}^{N(j)-1} \left\{ \frac{Y_{m(j)}}{W_0} (\alpha_{1, n(j)} + \alpha_{2, n(j)} - \alpha_{3, n(j)} - \alpha_{4, n(j)})_{m(j)} + \frac{Y_{m(j)+1}}{W_0} (\alpha_{3, n(j)} + \alpha_{4, n(j)})_{m(j)} \right\} \quad (29)$$

This equation can be rewritten in the form:

$$\cos \theta_{m(j)} = \sum_{N(j)=N(i)}^{N(j)} \sum_{m(j)=0}^{N(j)-1} \frac{Y_{m(j)}}{W_0} \beta_{m(j)} \quad (30)$$

where the coefficients $\beta_{m(j)}$ are as given below, with subscript (j) deleted.

$$\beta_{m=0}^{(1)} = (\alpha_{1m} + \alpha_{2m} - \alpha_{3m} - \alpha_{4m})_{m=0}$$

$$\beta_{m=1} = (\alpha_{3m} + \alpha_{4m})_{m=0} + (\alpha_{1m} + \alpha_{2m} - \alpha_{3m} - \alpha_{4m})_{m=1}$$

$$\beta_{m=n-2} = (\alpha_{3m} + \alpha_{4m})_{m=n-3} + (\alpha_{1m} + \alpha_{2m} - \alpha_{3m} - \alpha_{4m})_{m=n-2}$$

$$\beta_{m=n-1}^{(2)} = (\alpha_{3m} + \alpha_{4m})_{m=n-2} + \left(\frac{-\cos \frac{1}{2}(\theta_n - \theta_{n-1})}{2\pi} + \alpha_{2m} - \alpha_{4m} \right)_{m=n-1}$$

$$\beta_{m=n}^{(3)} = (\alpha_{4m})_{m=n-1} + (\alpha_{2m} - \alpha_{4m})_{m=n}$$

$$\beta_{m=n+1}^{(4)} = \left(\frac{\cos \frac{1}{2}(\theta_n - \theta_{n-1})}{2\pi} + \alpha_{4m} \right)_{m=n} + (\alpha_{1m} + \alpha_{2m} - \alpha_{3m} - \alpha_{4m})_{m=n+1}$$

$$\beta_{m=n+2} = (\alpha_{3m} + \alpha_{4m})_{m=n+1} + (\alpha_{1m} + \alpha_{2m} - \alpha_{3m} - \alpha_{4m})_{m=n+2}$$

$$\beta_{m=N(j)-3} = (\alpha_{3m} + \alpha_{4m})_{m=N(j)-4} + (\alpha_{1m} + \alpha_{2m} - \alpha_{3m} - \alpha_{4m})_{m=N(j)-3}$$

$$\beta_{m=N(j)-2}^{(5)} = (\alpha_{3m} + \alpha_{4m})_{m=N(j)-3} + (\alpha_{1m} + \alpha_{2m} - \alpha_{3m} - \alpha_{4m})_{m=N(j)-2} + T(\alpha_{3m} + \alpha_{4m})_{m=N(j)-1}$$

$$\beta_{m=N(j)-1} = (\alpha_{3m} + \alpha_{4m})_{m=N(j)-2} + (\alpha_{1m} + \alpha_{2m} - \alpha_{3m} - \alpha_{4m})_{m=N(j)-1}$$

$\beta_{m=0}^{(1)}$ is irregular because it is the first coefficient; $\beta_{m=n-1}^{(2)}$ is irregular because $m = n - 1$; $\beta_{m=n}^{(3)}$ is irregular because $m = n$; $\beta_{m=n+1}^{(4)}$ is irregular because $m = n + 1$; $\beta_{m=N(j)-2}^{(5)}$ is irregular because $T = Y_{N(j)} / Y_{N(j)-2}$

Equation (30) represents a set of $N-Q$ equations for $N-Q$ unknown values of $\gamma_{m(j)}$. The solution of this set of linear algebraic equations is obtained with the use of the digital computer subroutine DECOMP.⁶ The values of $\frac{\gamma_{m(j)}}{w_0}$ thus obtained, represents the dimensionless optimum strength distribution in the shed vortex sheet.

To compute the corresponding spanwise distribution of the bound vorticity Γ one has to integrate Eq. (2) numerically. First, the integration is performed along the fences starting with tip $N(2)$

$$\Gamma(j) = - \int_{\eta}^{\eta_{N(j)}} \gamma \, d\eta = \sum_{m(j)=N(j)-1}^{m(j) \text{ at wing root}} \frac{1}{2N} \left[\gamma_{m(j)} + \gamma_{m(j)+1} \right] \quad (31)$$

This integration is carried out along the wing, starting at the wing tip $N(1)$ and proceeding to the centerline. Every time a fence root is encountered the bound vortex on the wing experiences a step-like increase of magnitude $\Gamma(j)$

$$\Gamma(n) = \sum_{m(1)=N(1)-1}^{m(1) \text{ at 1st fence wing root}} \frac{1}{2N} \left[\gamma_{m(1)} + \gamma_{m(1)+1} \right] + \Gamma(2) + \sum_{m(1) \text{ is } 1 \text{ less than at 1st fence wing root}}^m \frac{1}{2N} \left[\gamma_{m(1)} + \gamma_{m(1)+1} \right] \quad (32)$$

The location of position n is shown in Fig. 6.

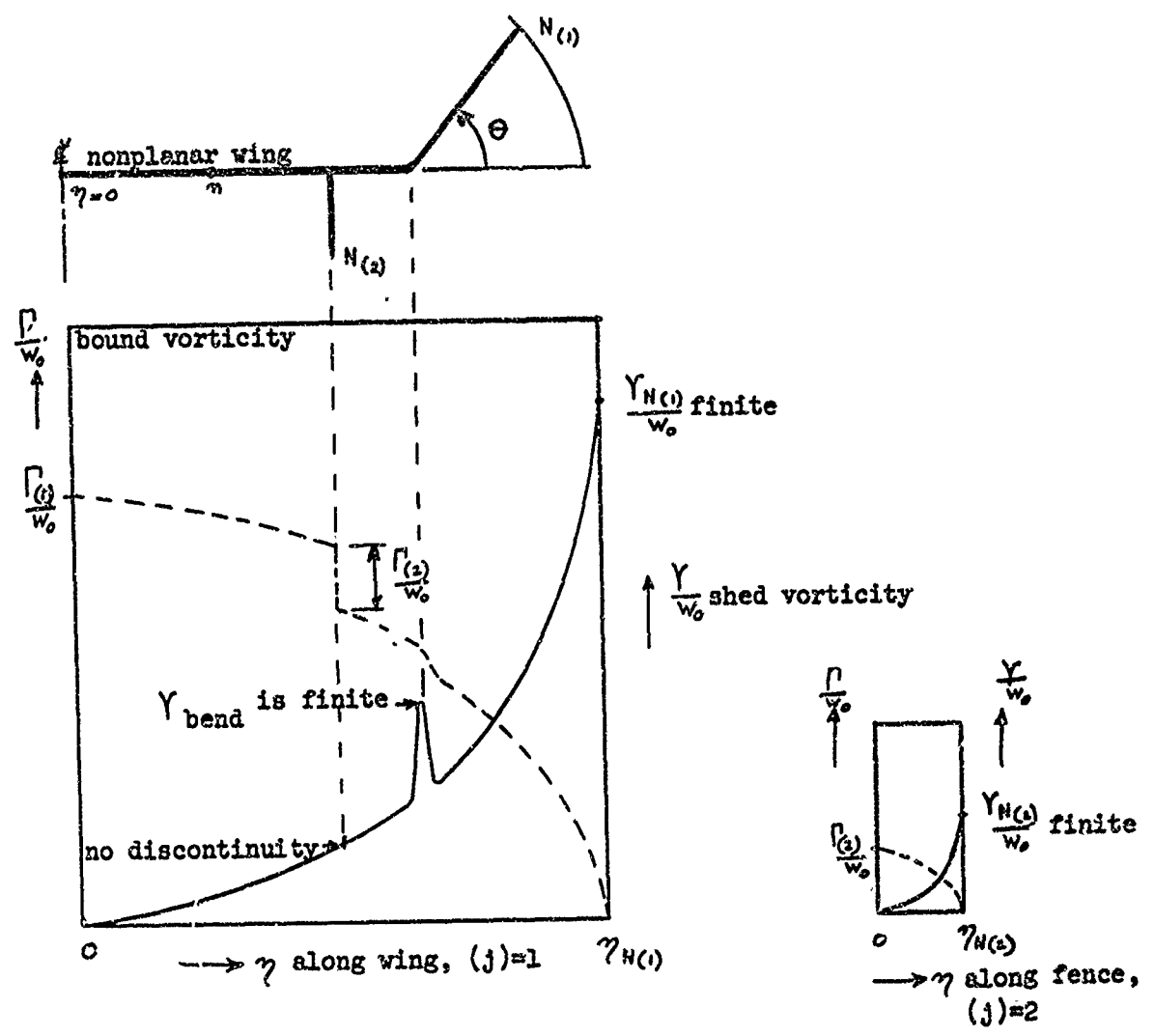


Figure 6: Effect of fences and bends on the vorticity.

RESULTS

The optimum loading computed with this method can be used to calculate the corresponding lift and induced drag on the wing. The lift \vec{L} is proportional to the vertical component of the force obtained from the vector product between \vec{V}_∞ and $\vec{\Gamma}$ and is:

$$\vec{L} = \int_{-\eta_{\max}}^{+\eta_{\max}} \rho_\infty (\vec{V}_\infty \times \vec{\Gamma}) \cos \theta \, d\eta \quad (33)$$

The induced drag \vec{D}_i is proportional to the vector product $\vec{w} \times \vec{\Gamma}$ using $\vec{w} \times \vec{\Gamma} = w_{\perp n} (\vec{n} \times \vec{\Gamma}) = w_o \cos \theta (\vec{n} \times \vec{\Gamma})$

$$\vec{D}_i = \int_{-\eta_{\max}}^{+\eta_{\max}} \rho_\infty w_o (\vec{n} \times \vec{\Gamma}) \cos \theta \, d\eta \quad (34)$$

The lift over induced drag ratio for wings with optimum loading is then:

$$\frac{L}{D_i} = \frac{V_\infty}{w_o} \quad (35)$$

To compare the L/D_i ratio between an elliptically loaded planar wing and an optimum loaded nonplanar wing, one should specify that both wings must have equal lift, and use Eq. (35) to define an induced drag efficiency factor k as:

$$k = \frac{\left[\frac{L}{D_i} \right]_{\text{nonplanar}}}{\left[\frac{L}{D_i} \right]_{\text{planar}}} = \frac{D_{i \text{ planar}}}{D_{i \text{ nonplanar}}} = \frac{w_o \text{ planar}}{w_o \text{ nonplanar}} \quad (36)$$

The following argument shows why the efficiency factor k is less than unity when the two wings being compared have equal total peripheral length. Both wings are chosen to have equal lift or:

$$\frac{L}{\rho_{\infty} V_{\infty}} = \left[\int_{-\gamma_{\max}}^{+\gamma_{\max}} \Gamma d\eta \right]_{\text{planar}} = \left[\int_{-\gamma_{\max}}^{+\gamma_{\max}} \Gamma \cos \theta d\eta \leq (\cos \theta)_{\max} \int_{-\gamma_{\max}}^{+\gamma_{\max}} \Gamma d\eta \right]_{\text{nonplanar}}$$

This inequality is given by the mean value theorem.

Defining an average bound vorticity $\bar{\Gamma} = \frac{1}{\gamma_{\max}} \int_0^{\gamma_{\max}} \Gamma d\eta$ then

$$\bar{\Gamma}_{\text{planar}} \leq (\cos \theta)_{\max} \bar{\Gamma}_{\text{nonplanar}}$$

or $\bar{\Gamma}_{\text{planar}} \leq \bar{\Gamma}_{\text{nonplanar}}$

If one defines an average shed vorticity $\bar{\gamma} = \frac{1}{\gamma_{\max}} \int_0^{\gamma_{\max}} \gamma d\eta$ then according to Eq. (2) $\bar{\Gamma} \sim \bar{\gamma} \cdot \gamma_{\max}$. From Eq. (30) it follows that $\bar{\gamma} \sim w_0$ or combining these results $\bar{\Gamma} \sim w_0 \cdot \gamma_{\max}$.

Assuming the proportionality constant to be of the same order of magnitude for both the planar and the nonplanar wing one obtains:

$$\left[w_0 \cdot \gamma_{\max} \right]_{\text{planar}} \leq \left[w_0 \cdot \gamma_{\max} \right]_{\text{nonplanar}}$$

$$w_0'_{\text{planar}} \leq w_0'_{\text{nonplanar}}$$

$$k = \frac{w_0'_{\text{planar}}}{w_0'_{\text{nonplanar}}} \leq 1.0$$

This is the definition of the efficiency factor used.

The effect of a dihedral angle on the efficiency factor $k \leq 1.0$ is shown in Fig. 7. Both planar and nonplanar wings have the same total peripheral length and consequently the same area and skin friction drag. The nonplanar wing has a shorter span but its performance is worse because of the lower lift over induced drag ratio. Seemingly contradicting results are found in Ref. 2, where the efficiency factor $k \geq 1.0$, because Lundry has compared the nonplanar wing with a planar wing of equal span instead of equal peripheral length. Under these conditions the area and the skin friction of the nonplanar wing is larger than that of the planar wing but its performance is better because it has a higher lift over induced drag ratio than the planar wing. The optimum loading computed in this paper is in exact agreement with the results obtained by Lundry in Ref. 2, except the efficiency factor k is defined differently (see Fig. 7).

In conclusion it can be said that if the span is the limiting factor then it may be advantageous to use nonplanar wings with dihedral angle and fences. However, if the total peripheral wing length is limited, then the planar wing is always the most desirable configuration with the highest lift over drag ratio.

The numerical solution was tested for a simple nonplanar wing with a planar center section and a dihedral angle Θ , which is constant for the outer portion starting at η_0 . The optimum vorticity distribution in the shed vortex sheet is shown in dimensionless form in Figs. 8 and 9. There is a sharp increase in γ near the bend in the wing, $N = 100$ in this calculation. The ratio between the bound vorticity $\bar{\Gamma}$ and its average value $\bar{\Gamma}$ is shown in Figs. 10 and 11. The effect of the dihedral angle on the required increase in the optimum loading is shown in Figs. 12 and 13.

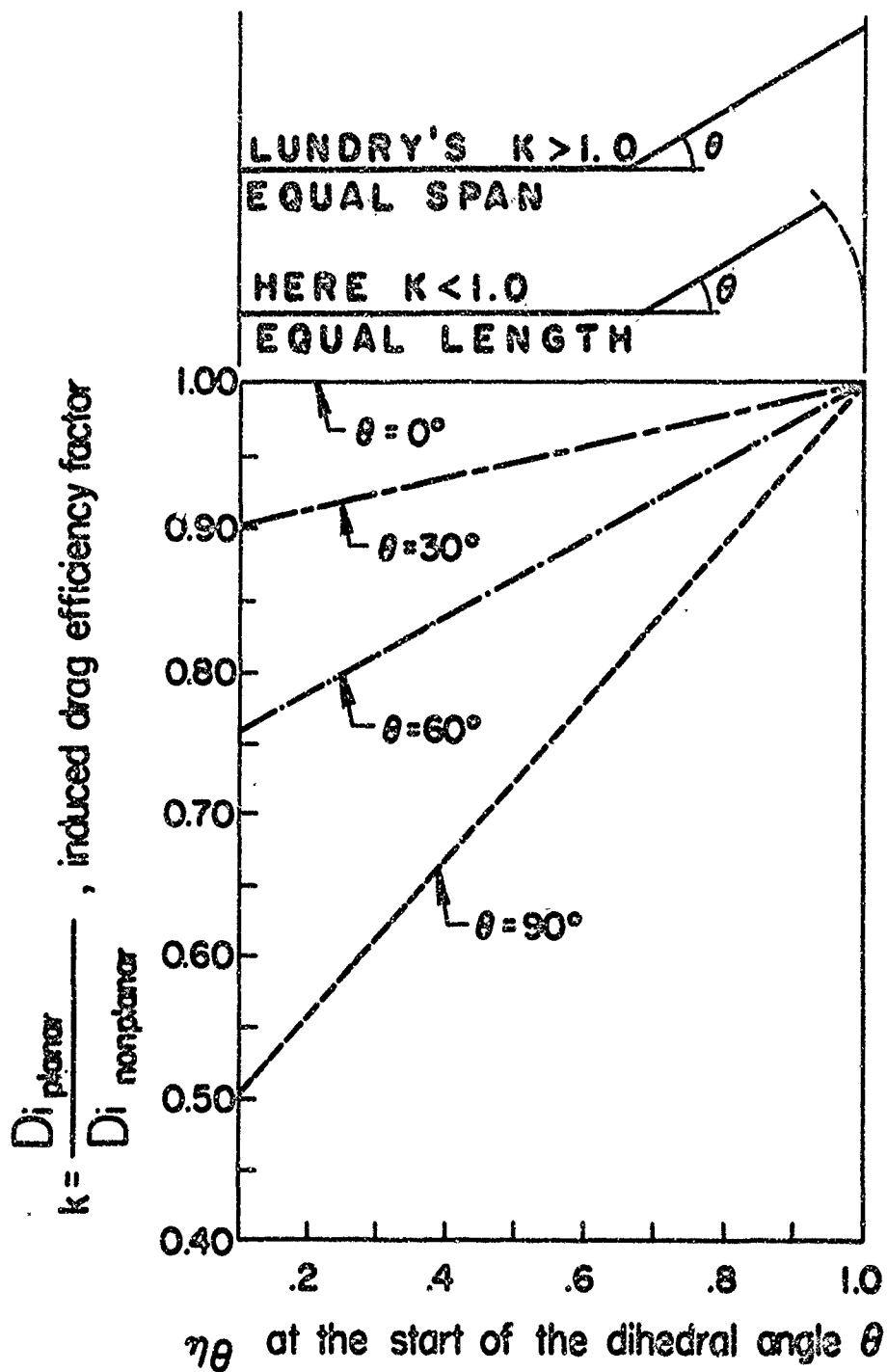


Figure 7: Induced drag efficiency.

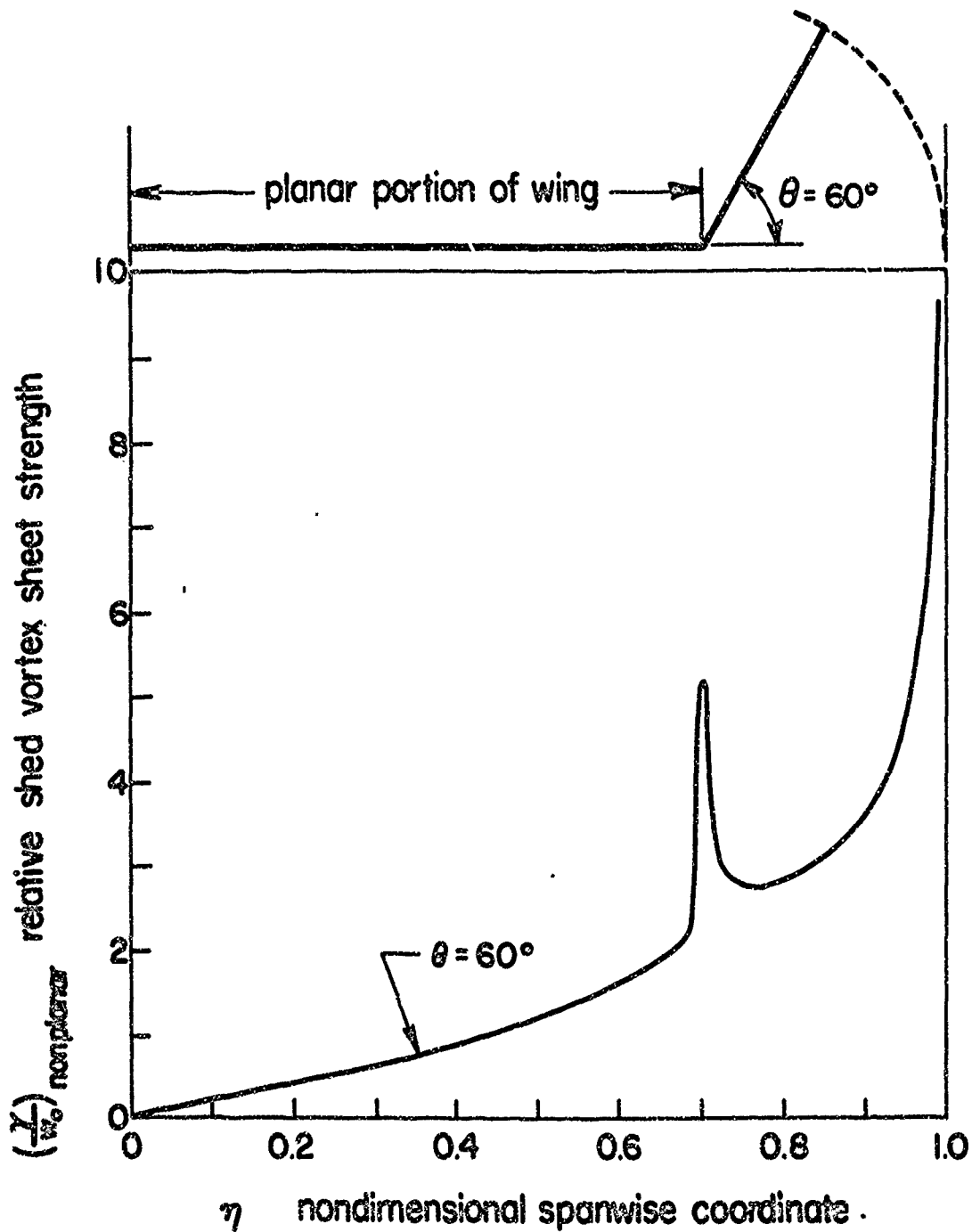


Figure 8: Optimum vorticity distribution in the Trefftz plane.

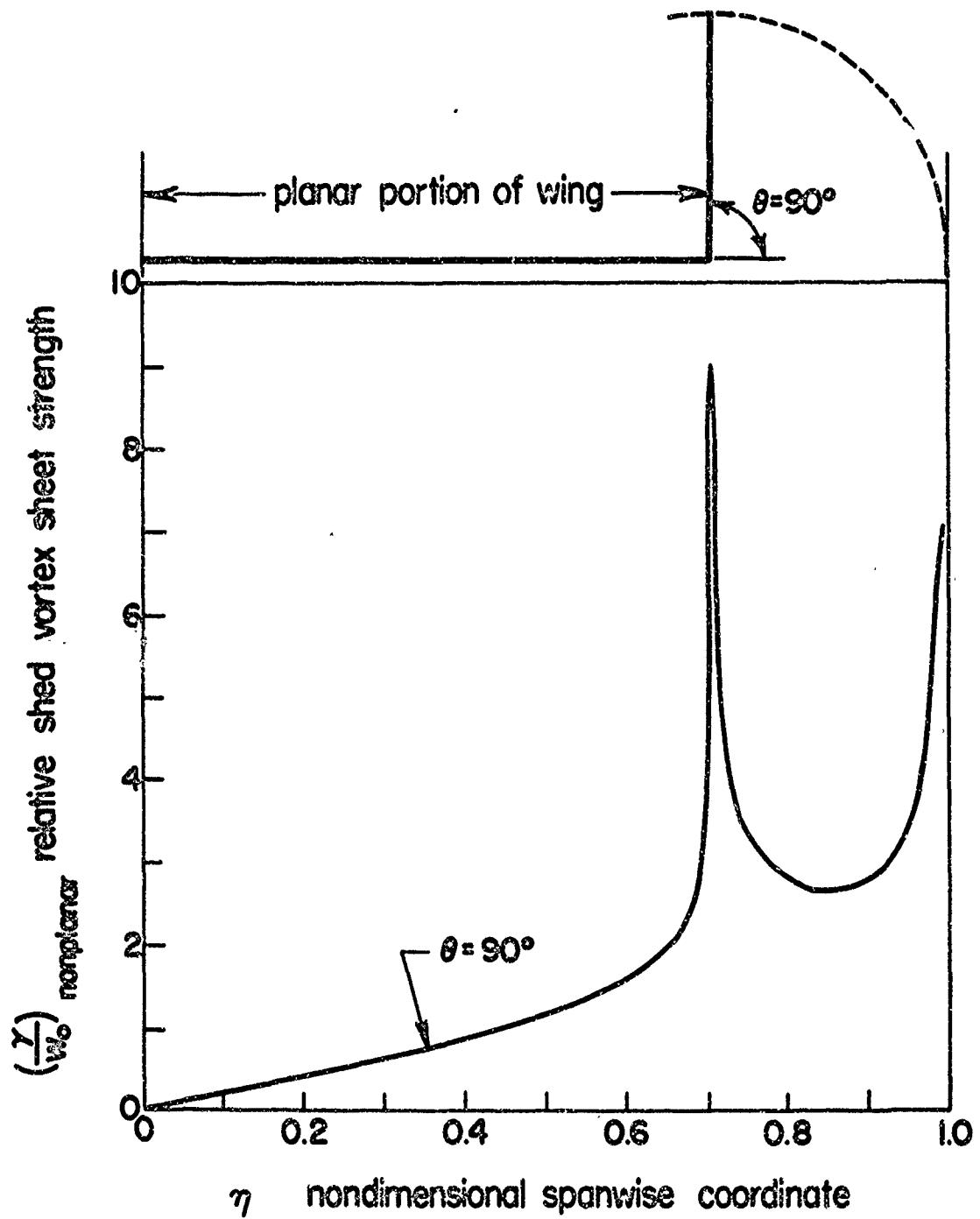


Figure 9: Optimum vorticity distribution in the Trefftz plane.

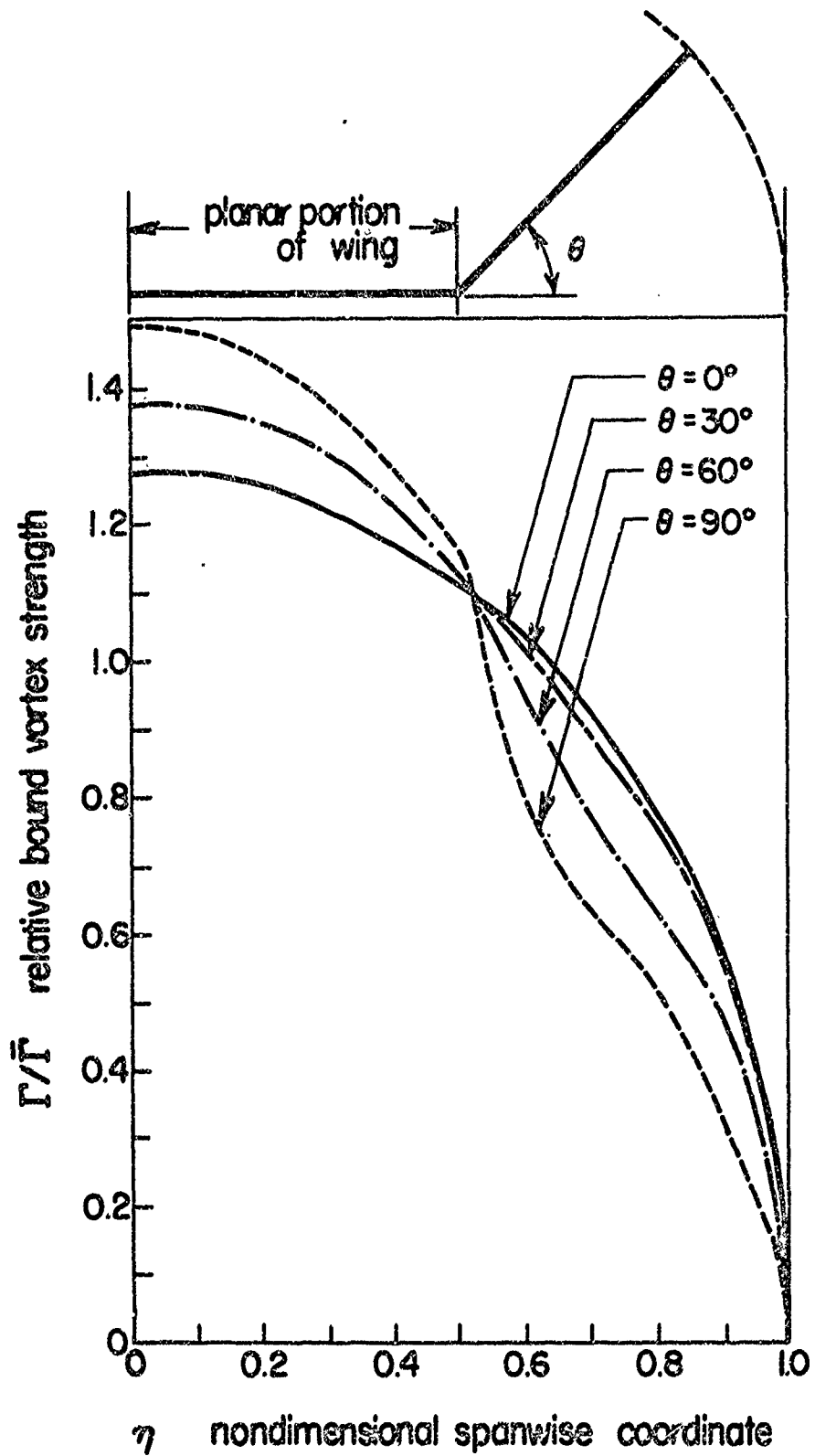


Figure 10: Optimum bound vorticity on the wing.

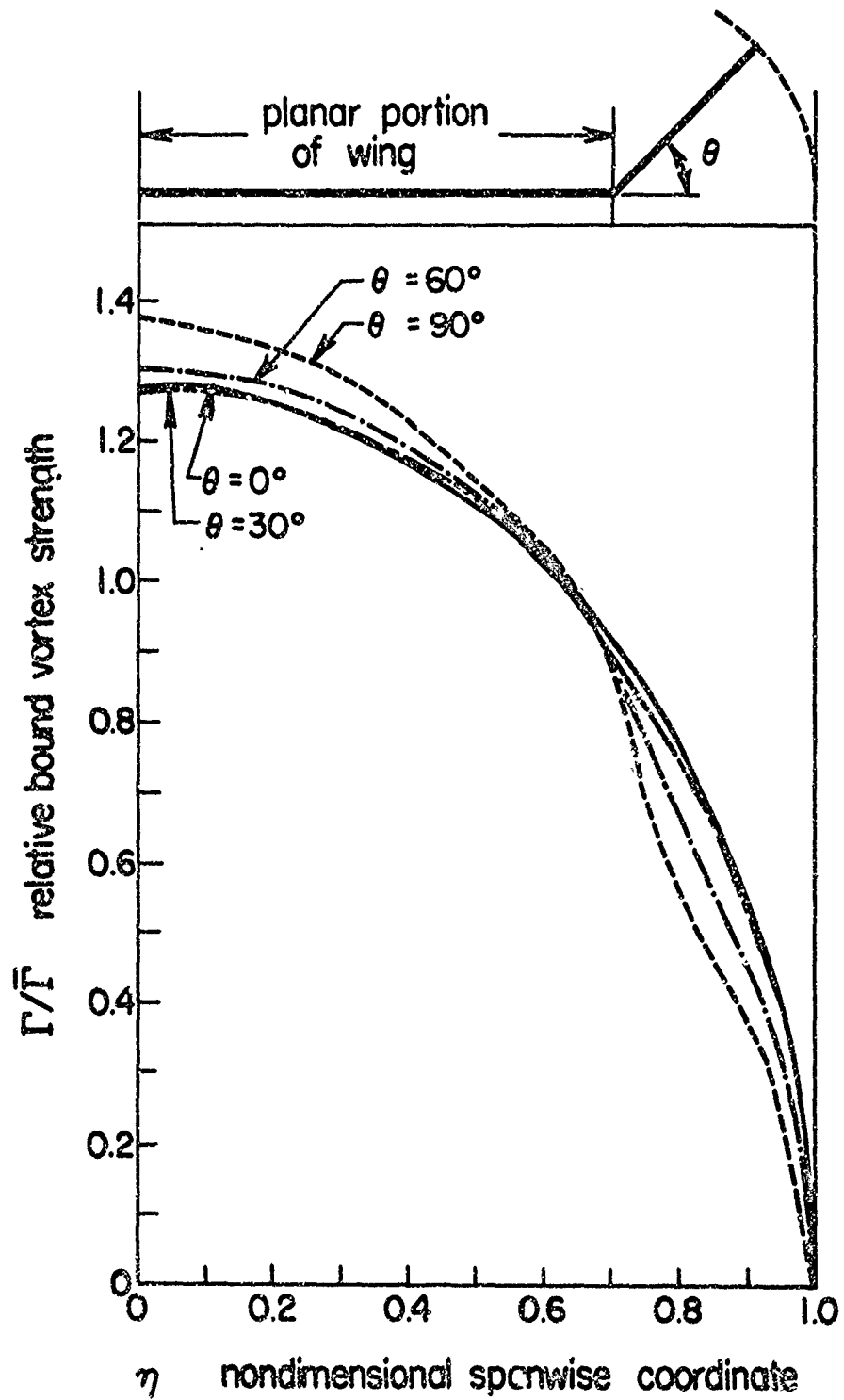


Figure 11: Optimum bound vorticity on the wing.

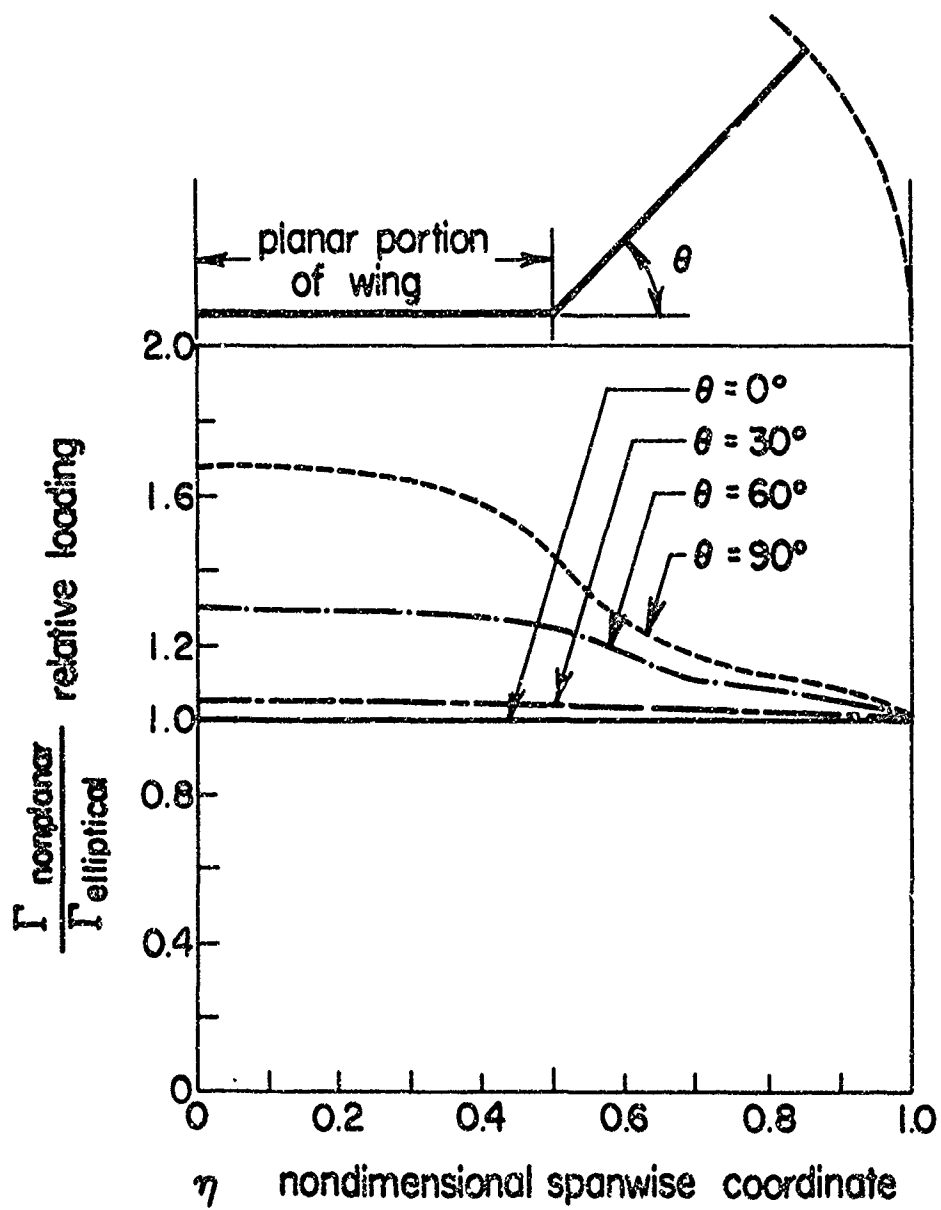


Figure 12: Relative bound vorticity.

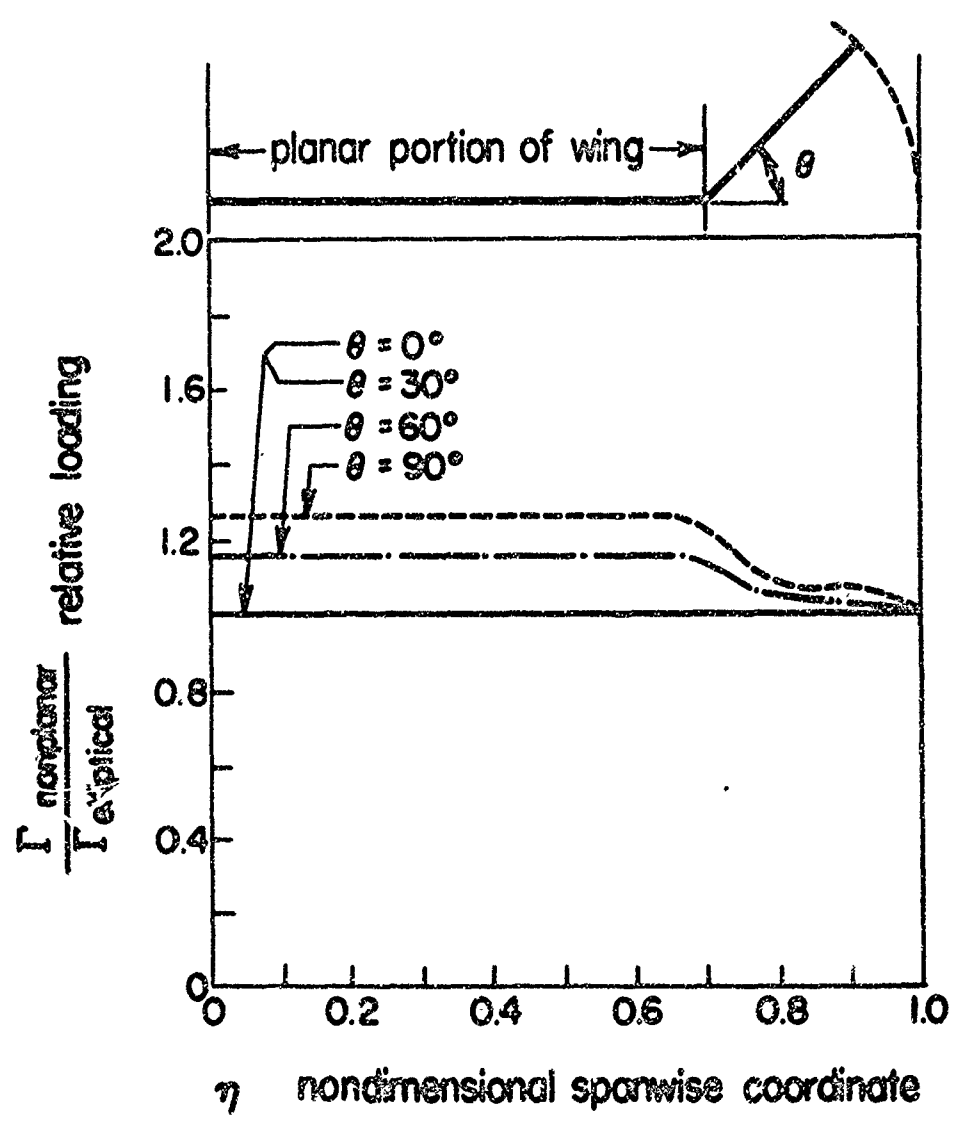


Figure 13 : Relative bound vorticity.

CONCLUSIONS

The results of this numerical technique have been compared to the conformal mapping solution as presented by Lundry² in his configuration 5 and excellent agreement was obtained.

The numerical solution used in this program takes little computer time and is suitable for computer optimization of fence position, size, and dihedral angle. Only the β matrix coefficients that belong to the fence in question need to be recomputed for each configuration change.

The step size $\Delta\eta$ need not be constant = $1/N$ as was used here. Wherever $1/N$ appears in the equations it can be replaced by the local magnitude of $\Delta\eta$ used.

The input data for the computer should include the total number of vortex sheet segments N and their coordinates x_n , y_n and dihedral angle θ_n . In addition $\Delta\eta_n$ must be specified for each station n , if the segments are not of equal length.

It is noteworthy to realize that Lundry² compared his nonplanar wing to an elliptically loaded planar wing with the same span and found the induced drag efficiency factor $k \geq 1.0$. Consequently, when the span is the limiting factor it is advantageous to use a nonplanar wing. In this analysis, the nonplanar wing is compared to an elliptically loaded planar wing with the same peripheral length. The induced drag coefficient k was found to be ≤ 1.0 , and consequently if the total peripheral length is a limiting factor it is advantageous to use a planar wing. Either method can be used to find the optimum loading of a nonplanar wing.

REFERENCES

1. Munk, M.M. "The Minimum Induced Drag of Airfoils," NACA Report No. 121, 1921.
2. Lundry, J.L. "A Numerical Solution for the Minimum Induced Drag and the Corresponding Loading of Nonplanar Wings," NASA CR-1218, 1968.
3. Cone, C.D., Jr. "The Theory of Induced Lift and Minimum Induced Drag of Nonplanar Lifting Systems," NASA TR-139, 1962.
4. Blackwell, J.A., Jr. "A Finite-Step Method for Calculation of Theoretical Load Distribution for Arbitrary Lifting-Surface Arrangements at Subsonic Speeds," NASA TN D-5335, July 1969.
5. Robert, S.C. "An Investigation of End Plates to Reduce the Drag of Planar Wings," Mississippi State University USAAVLABS TR-65-79, 1966.
6. Forsythe, G. and C. Moler "Computer Solution of Linear Algebraic Systems," Prentice-Hall, New York, 1967.

APPENDIX A

The integration of the coefficients

$$\alpha_{1m,m} = \frac{1}{2\pi} \int_0^{\Delta\eta} \frac{R'_{n,m}}{(r'_{n,m})^2} dh \quad (12)$$

$$\alpha_{2m,m} = \frac{1}{2\pi} \int_0^{\Delta\eta} \frac{-R''_{n,m}}{(r''_{n,m})^2} dh \quad (13)$$

$$\alpha_{3m,m} = \frac{1}{2\pi} \int_0^{\Delta\eta} \frac{h}{\Delta\eta} \left[\frac{R'_{n,m}}{(r'_{n,m})^2} \right] dh \quad (14)$$

$$\alpha_{4m,m} = \frac{1}{2\pi} \int_0^{\Delta\eta} \frac{h}{\Delta\eta} \left[\frac{-R''_{n,m}}{(r''_{n,m})^2} \right] dh \quad (15)$$

Equations 8a and 8b , can be written as:

$$R'_{n,m} = (A + hB)_{n,m}$$

$$\text{where } A_{n,m} = (x_m - x_n) \cos \theta_m + (y_m - y_n) \sin \theta_m \quad (38)$$

$$\text{and } B_{n,m} = \cos \theta_m \cos \theta_n + \sin \theta_m \sin \theta_n \quad (39)$$

$$R''_{n,m} = (D + hE)_{n,m}$$

$$\text{where } D_{n,m} = -(x_m + x_n) \cos \theta_m + (y_m - y_n) \sin \theta_m \quad (40)$$

$$\text{and } E_{n,m} = -\cos \theta_m \cos \theta_n + \sin \theta_m \sin \theta_n \quad (41)$$

APPENDIX A

Equations 9a and 9b can be rewritten as:

$$(r'_{n,m})^2 = (h^2 + hF + G)_{n,m}$$

$$\text{where } F_{n,m} = 2 \cos \theta_m (x_m - x_n) + 2 \sin \theta_m (y_m - y_n) \quad (42)$$

$$\text{and } G_{n,m} = (x_m - x_n)^2 + (y_m - y_n)^2 \quad (43)$$

$$(r''_{n,m})^2 = (h^2 + hJ + k)_{n,m}$$

$$\text{where } J_{n,m} = 2 \cos \theta_m (x_m + x_n) + 2 \sin \theta_m (y_m - y_n) \quad (44)$$

$$\text{and } K_{n,m} = (x_m + x_n)^2 + (y_m - y_n)^2 \quad (45)$$

Inserting these expressions in Eqs. 12-15 gives:

$$\alpha_{1n,m} = \frac{1}{2\pi} \int_0^{\Delta\eta} \left(\frac{A + hB}{h^2 + hF + G} \right)_{n,m} dh$$

$$\alpha_{2n,m} = \frac{1}{2\pi} \int_0^{\Delta\eta} - \left(\frac{D + hE}{h^2 + hJ + k} \right)_{n,m} dh$$

$$\alpha_{3n,m} = \frac{1}{2\pi} \int_0^{\Delta\eta} \frac{1}{\Delta\eta} \left(\frac{hA + h^2B}{h^2 + hF + G} \right)_{n,m} dh$$

$$\alpha_{4n,m} = \frac{1}{2\pi} \int_0^{\Delta\eta} - \frac{1}{\Delta\eta} \left(\frac{hD + h^2E}{h^2 + hJ + k} \right)_{n,m} dh$$

APPENDIX A

The denominators are of the type $ah^2 + bh + c = H$, with $4ac \gg b^2$

This is because: $4G_{n,m} \gg F_{n,m}^2$ and $4K_{n,m} \gg J_{n,m}^2$

Proof for $4G_{n,m} \gg F_{n,m}^2$

$$\begin{aligned}
 4 \left[(x_m - x_n)^2 + (y_m - y_n)^2 \right] &\gg 4 \left[(x_m - x_n)^2 \cos^2 \theta_m + (y_m - y_n)^2 \sin^2 \theta_m + \right. \\
 &\quad \left. 2(x_m - x_n)(y_m - y_n) \sin \theta_m \cos \theta_m \right] \\
 0 &\gg \left[-(x_m - x_n)^2 \sin^2 \theta_m - (y_m - y_n)^2 \cos^2 \theta_m + \right. \\
 &\quad \left. 2(x_m - x_n)(y_m - y_n) \sin \theta_m \cos \theta_m \right] \\
 0 &\gg - \left[(x_m - x_n) \sin \theta_m - (y_m - y_n) \cos \theta_m \right]^2
 \end{aligned}$$

When $4ac - b^2 > 0$ then: $\int \frac{dh}{H} = \frac{2}{(4ac - b^2)^{1/2}} \tan^{-1} \frac{2ah + b}{(4ac - b^2)^{1/2}}$

When $4ac - b^2 = 0$ then: $\int \frac{dh}{H} = \frac{-2}{(2ah + b)}$

for all values of $4ac - b^2$

$$\int \frac{h dh}{H} = \frac{1}{2a} \ln |H| - \frac{b}{2a} \int \frac{dh}{H}$$

$$\int \frac{h^2 dh}{H} = \frac{h}{a} - \frac{b}{2a^2} \ln |H| + \frac{b^2 - 2ac}{2a^2} \int \frac{dh}{H}$$

APPENDIX A

for $4G_{n,m} - F_{n,m}^2 > 0$ put $\int_0^{\Delta\eta} \frac{dh}{H} = P$ and $\Delta\eta = \frac{1}{N}$

$$P_{n,m} = \frac{2}{(4G - F^2)_{n,m}^{1/2}} \left\{ \tan^{-1} \frac{\frac{2}{N} + F}{(4G - F^2)_{n,m}^{1/2}} - \tan^{-1} \frac{F}{(4G - F^2)_{n,m}^{1/2}} \right\} \quad (46a)$$

for $4G_{n,m} - F_{n,m}^2 = 0$ or very small

$$P_{n,m} = \left\{ \frac{2}{F} - \frac{2}{\frac{2}{N} + F} \right\}_{n,m} \quad (46b)$$

for $4J_{n,m} - k_{n,m}^2 > 0$ put $\int_0^{\Delta\eta} \frac{dh}{H} = S$ and $\Delta\eta = \frac{1}{N}$

$$S_{n,m} = \frac{2}{(4J - k^2)_{n,m}^{1/2}} \left\{ \tan^{-1} \frac{\frac{2}{N} + k}{(4J - k^2)_{n,m}^{1/2}} - \tan^{-1} \frac{k}{(4J - k^2)_{n,m}^{1/2}} \right\} \quad (47a)$$

for $4J_{n,m} - k_{n,m}^2 = 0$ or very small

$$S_{n,m} = \left\{ \frac{2}{k} - \frac{2}{\frac{2}{N} + k} \right\}_{n,m} \quad (47b)$$

$$\alpha_{1n,m} = \frac{1}{2\pi} \left[P \left(A - \frac{BF}{2} \right) + \frac{B}{2} \ln \left| \frac{1}{GN^2} + \frac{F}{GN} + 1 \right| \right]_{n,m} \quad (48)$$

$$\alpha_{2n,m} = \frac{-1}{2\pi} \left[S \left(D - \frac{EJ}{2} \right) + \frac{E}{2} \ln \left| \frac{1}{KN^2} + \frac{J}{KN} + 1 \right| \right]_{n,m} \quad (49)$$

$$\alpha_{3n,m} = \frac{N}{2\pi} \left[P \left(\frac{BF^2 - 2BG - AF}{2} \right) + \left(\frac{A - BF}{2} \right) \ln \left| \frac{1}{GN^2} + \frac{F}{GN} + 1 \right| + \frac{B}{N} \right]_{n,m} \quad (50)$$

$$\alpha_{4n,m} = \frac{-N}{2\pi} \left[S \left(\frac{EJ^2 - 2EK - DJ}{2} \right) + \left(\frac{D - EJ}{2} \right) \ln \left| \frac{1}{KN^2} + \frac{J}{KN} + 1 \right| + \frac{E}{N} \right]_{n,m} \quad (51)$$

APPENDIX B

The special case is given where $m = n$ and $m = n-1$. Under this special condition the normal component of the induced velocity at n is evaluated at the end of a vortex sheet segment with finite strength γ_n ; consequently the contribution to $\Delta W_{\perp n, m}$ from the adjacent segments on the right hand side of the vortex sheet, as given by the coefficients α_1 and α_2 will be positive and infinite for $m = n$ where $\alpha_{1, m, m=n} = +\infty$ and be negative and infinite for $m = n-1$ where $\alpha_{1, m, m=n-1} = -\infty$. This infinite velocity can be avoided if the integration is carried out over both vortex sheet segments simultaneously as shown in Fig. 14.

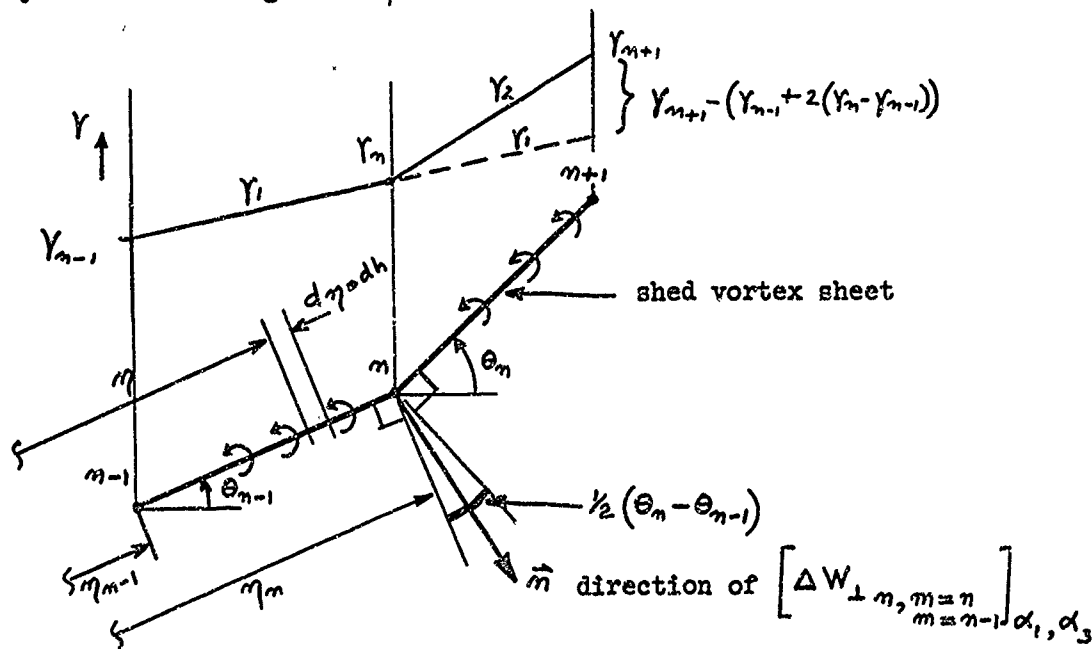


Figure 14: Vortex sheet segments for $m = n$ and $m = n-1$.

When the dihedral angle $\theta_n \neq \theta_{n-1}$, then there is a bend in the vortex sheet and the corresponding exact solution of $\gamma_{bend} = \infty$.

APPENDIX B

In order to smooth out the bends and avoid the necessity for γ to go to infinity, one can choose the unit normal vector \vec{n} along the average normal to the two segments as is shown in Fig. 14.

Applying the Biot Savart law as in Eq. (8) gives the velocity component $\left[\Delta W_{\perp n, \substack{m=n-1 \\ m=n}} \right]_{\alpha_1, \alpha_3}$ induced at n by both neighboring vortex sheet segments, but not including the contribution from the left hand side of the vortex sheet as given by α_2 and α_3 .

$$\left[\Delta W_{\perp n, \substack{m=n-1 \\ m=n}} \right]_{\alpha_1, \alpha_3} = \int_{\eta_{n-1}}^{\eta_{n+1}} \frac{\gamma}{2\pi(\eta - \eta_m)^2} \left[\vec{n} \cdot (\vec{\eta} - \vec{\eta}_m \times \vec{z}) \right] d\eta$$

where $\frac{\vec{n} \cdot (\vec{\eta} - \vec{\eta}_m \times \vec{z})}{(\eta - \eta_m)^2} = \frac{\cos k(\theta_n - \theta_{n-1})}{\eta - \eta_m}$

Linearizing the vorticity distribution as in Eq. (10) produced a discontinuity in γ at station n . This vorticity distribution can be replaced by one continuous function over both segments γ_1 , and by one distribution γ_2 which goes to zero at station n so that $\gamma = \gamma_1 + \gamma_2$ as shown in Fig. 14.

$$\text{for } \eta_{n-1} < \eta < \eta_{n+1} \quad \gamma_1 = \gamma_{n-1} + (\gamma_n - \gamma_{n-1}) \frac{\eta - \eta_{n-1}}{\eta_n - \eta_{n-1}}$$

$$\text{for } \eta_{n-1} < \eta < \eta_n \quad \gamma_2 = 0$$

$$\text{for } \eta_n < \eta < \eta_{n+1} \quad \gamma_2 = \left[\gamma_{n+1} - (\gamma_{n-1} + 2(\gamma_n - \gamma_{n-1})) \right] \frac{\eta - \eta_n}{\eta_{n+1} - \eta_n}$$

$$\text{or } \left[\Delta W_{\perp n, \substack{m=n-1 \\ m=n}} \right]_{\alpha_1, \alpha_3} = \frac{\cos k(\theta_n - \theta_{n-1})}{2\pi} \left[\int_{\eta_{n-1}}^{\eta_{n+1}} \frac{\gamma_1}{\eta - \eta_m} + \int_{\eta_n}^{\eta_{n+1}} \frac{\gamma_2}{\eta - \eta_m} \right]$$

APPENDIX B

using $\int \frac{d\eta}{\eta-a} = \ln|\eta-a|$ and $\int \frac{\eta-a}{\eta-b} d\eta = \eta + (b-a) \ln|\eta-b|$

gives

$$\left[\Delta W_{\perp n, \substack{m=n-1 \\ m=n}} \right]_{\alpha_1, \alpha_3} = \frac{\cos \frac{1}{2}(\theta_n - \theta_{n-1})}{2\pi} \left[Y_{m=n+1} - Y_{m=n-1} \right] \quad (52)$$

As a result of this, one can write with the use of Eq. (11), the contribution of the right hand side of the vortex sheet as:

$$\begin{aligned} \left[\Delta W_{\perp n, \substack{m=n-1 \\ m=n}} \right]_{\alpha_1, \alpha_3} &= Y_{m=n-1} \alpha_{1, n, m=n-1} + (Y_{m=n} - Y_{m=n-1}) \alpha_{3, n, m=n-1} \\ &\quad Y_{m=n} \alpha_{1, n, m=n} + (Y_{m=n+1} - Y_{m=n}) \alpha_{3, n, m=n} \end{aligned}$$

Equating this to Eq. (52) gives the coefficients:

$$\alpha_{1, n, m=n-1} = - \frac{\cos \frac{1}{2}(\theta_n - \theta_{n-1})}{2\pi} \quad (53)$$

$$\alpha_{1, n, m=n} = + \frac{\cos \frac{1}{2}(\theta_n - \theta_{n-1})}{2\pi} \quad (54)$$

$$\alpha_{3, n, m=n-1} = 0 \quad (55)$$

$$\alpha_{3, n, m=n} = + \frac{\cos \frac{1}{2}(\theta_n - \theta_{n-1})}{2\pi} \quad (56)$$

Unclassified

Security Classification

DOCUMENT CONTROL DATA - R & D

Security classification of title, body of abstract and indexing annotation must be entered when the overall report is classified

1. ORIGINATING ACTIVITY (Corporate author) West Virginia University Department of Aerospace Engineering Morgantown, West Virginia 26506		2a. REPORT SECURITY CLASSIFICATION Unclassified	
		2b. GROUP	
3. REPORT TITLE Optimum Loading on Nonplanar Wings at Minimum Induced Drag			
4. DESCRIPTIVE NOTES (Type of report and, inclusive dates) Scientific			
5. AUTHOR(S) (First name, middle initial, last name) John L. Loth and Robert E. Boyle			
6. REPORT DATE August 1, 1969		7a. TOTAL NO. OF PAGES 37	7b. NO. OF REFS 6
8a. CONTRACT OR GRANT NO. N00014-68-A-0512		9a. ORIGINATOR'S REPORT NUMBER(S) Aerospace Engineering TR-19	
b. PROJECT NO. NR 215-163			
c. Project THEMIS		9b. OTHER REPORT NO(S) (Any other numbers that may be assigned this report)	
d.			
10. DISTRIBUTION STATEMENT Distribution of this Document is Unlimited			
11. SUPPLEMENTARY NOTES		12. SPONSORING MILITARY ACTIVITY Office of Naval Research Naval Application and Analysis Division Aeronautics Branch	
13. ABSTRACT A numerical technique has been developed for computing the optimum spanwise load distribution on nonplanar wings of arbitrary shape. Munk's criterion for minimum induced drag was used. The problem is solved in the two-dimensional Trefftz plane. The two-dimensional shed vortex sheet is assumed to have the same shape as the nonplanar wing from which it has been shed. The vortex sheet in the Trefftz plane is subdivided into 2N segments. Each vortex sheet segment is assumed to have a linear vorticity distribution. The velocity induced at N-Q stations is determined with the Biot-Savart law. The problem is then reduced to solving a set of linear algebraic equations. The technique has been applied to nonplanar wings with various dihedral angles and locations of the nonplanar wing sections. It was concluded that, if the span is the limiting factor then it may be advantageous to use nonplanar wings. On the other hand, if the wing total peripheral length is limited, then the planar wing is always the most desirable configuration, with the highest lift over drag ratio.			

Unclassified

Security Classification

14 KEY WORDS	LINK A		LINK B		LINK C	
	ROLE	WT	ROLE	WT	ROLE	WT
Fixed Wing						
Induced Drag						
Induced Velocity						
Nonplanar Wing						
Optimum Wing						
Shed Vortex Sheet						

DU FORM 1473 (BACK)
1 NOV 68

S/H 0102-014-5800

Unclassified

Security Classification

A-51409